Controllable Manipulation of Wi-Fi Signals Using Tunable Metasurface

SHUANG Ya[①] LI Li[②] WANG Zhuo[①] WEI Menglin[①] LI Lianlin*[①]

[①](*State Key Laboratory of Advanced Optical Communication Systems and Networks*, *Department of Electronics*, *Peking University*, *Beijing* 100871, *China*)

[②](*Beijing Aerospace Measurement & Control Technology CO., LTD.*, *Beijing* 100871, *China*)

Abstract: In this paper, we propose the utilization of a programmable metasurface for flexibly manipulating ambient Wi-Fi signals. First, we propose a new and efficient optimization algorithm CWGS (Complex Weighted Gerchberg-Saxton), which is based on an electromagnetic scattering model of the metasurface. The proposed algorithm quickly redesigns the complex amplitude distribution of the Wi-Fi field bounced off the programmable metasurface to enhance the Wi-Fi signals at desired locations significantly. Second, we fabricated a large-scale programmable metasurface that operates at the 2.4 GHz frequency band. We conducted several experiments using the fabricated metasurface to verify the proposed optimization algorithm's feasibility and effectiveness. Both the theoretical and experimental results show that the programmable metasurface can dynamically boost Wi-Fi signals at multiple locations. Besides, we experimentally verified that using the developed strategy could improve the Wi-Fi signals by 23.5 dB. The results of our work improve the usability and practicality of the programmable metasurface in real-world applications and pave the way for wireless communications, future smart homes, and other applications.

Key words: Commodity Wi-Fi signals; Programmable coding metasurface; Spatial energy allocation

DOI: 10.12000/JR21012

Reference format: SHUANG Ya, LI Li, WANG Zhuo, *et al*. Controllable manipulation of Wi-Fi signals using tunable metasurface[J]. *Journal of Radars*, 2021, 10(2): 313–325. DOI: 10.12000/JR21012.

引用格式：双雅, 李力, 王卓, 等. 基于可编程超表面的Wi-Fi信号调控[J]. 雷达学报, 2021, 10(2): 313–325. DOI: 10.12000/JR21012.

基于可编程超表面的Wi-Fi信号调控

双 雅[①] 李 力[②] 王 卓[①] 魏梦麟[①] 李廉林*[①]

[①](北京大学信息科学技术学院 北京 100871)

[②](北京航天测控技术有限公司 北京 100871)

摘 要：可编程超表面是由可调谐的单元在二维平面上组成的平面阵列，具有任意、动态操控电磁波波前的能力，是微波领域前沿研究方向之一。尽管目前基于可编程超表面的电磁调控研究已取得丰硕进展，但是现有技术都需要采用专用发射源主动馈电超表面，这不仅增加了实际系统的复杂性和成本，而且在一定程度上限制了这些技术在现实环境中的应用。因此，该文提出了一种利用可编程超表面灵活调控周围Wi-Fi信号的方法，并通过理论和实验证明了其对Wi-Fi信号的优越调控性能。首先，该文首次提出一种基于可编程超表面散射模型的高效优化算法CWGS，该算法可以重新设计可编程超表面散射场的复振幅分布，从而实现指定位置处的Wi-Fi信号显著增强。其次，该文制作了一款工作频率为2.4 GHz的大规模可编程超表面，并基于该超表面实验验证了优化算法应用于Wi-Fi信号增强调控的可行性和有效性。理论和实验结果均证明，可编程超表面可以在多个位置处实现Wi-Fi信号的动态增强。实验结果表明，经可编程超表面调控后的Wi-Fi信号强度提高了23.5 dB。该文提出的方法提高了可编程超表面在实际应用中的可用性和实用性，有望为无线通信、未来智能家居等领域开辟新的道路。

Manuscript received February 19, 2021; Revised April 02, 2021; Published online April 26, 2021.

*Communication Author: LI Lianlin

E-mail: lianlin.li@pku.edu.cn

Foundation Item: The National Key Research and Development Program of China (2017YFA0700203)

Corresponding Editor: LI Long

关键词：商用Wi-Fi 信号；可编码超表面；空间能量分配
中图分类号：TN82 文献标识码：A 文章编号：2095-283X(2021)02-0313-13

1 Introduction

Radio-Frequency (RF) signals, extending human's senses in a contactless way, hold ever-increasing potentials in the modern society due to the unique capability of working in all-weather all-day and through-the-opaque conditions. Many advanced technologies have been proposed to achieve what was thought to be impossible by exploring RF signals, especially assisted with the extraordinarily promising programmable metasurfaces. Programmable metasurfaces, which are composed of an array of electronically-controllable digital meta-atoms, have been demonstrated to be powerful in arbitrarily and dynamically manipulating Electro Magnetic (EM) wavefronts[1–11]. Until now, fruitful progress based on programmable metasurfaces have been reported, for instance, wide-angle beam scanner[1], reconfigurable metasurface holograms[2,3], machine-learning imager[4], tunable near-field focusing[6,8,9], wireless power transfer[11,12], programmable wireless communication[13], and so on.

However, these techniques work in an active manner in the sense that cooperative RF signals transmitted by a dedicated source are required to actively feed the metasurfaces, which not only increases the complexity and cost of practical systems but also limits the real-world applications of these techniques to some extent, especially in indoor environments. Moreover, when artificially manipulating the scattering field or radiation field of metasurfaces, only the field's amplitude patterns have been carefully considered in the aforementioned works, leaving the important phase information of field to be ignored. Therefore, it's urgent to explore a both innovative and practical strategy to making full use of EM waves with the aid of programmable metasurfaces, which could be more useful in realistic environments. Then, we notice that there are increasing interests in developing advanced and green techniques by utilizing the pervasive Wi-Fi signals due to the widespread popularity of wireless local area networks, which includes Wi-Fi-band wireless energy harvesting[14], human behavior sensing whatever people are in a line-of sight or non-line-of-sight scenario[15–18], three-dimensional Wi-Fi holography imaging[19,20], and intelligent imaging and recognition in Wi-Fi band[21].

Inspired by the idea of developing green techniques, we would like to demonstrate an efficient approach that ambient Wi-Fi signals can be tailored flexibly assisted with programmable metasurfaces, which could be considered as a passive strategy compared with these existing works[1–11,13,22–25]. In this work, we primarily focus on the theoretical and experimental investigations of the proposed strategy that commodity Wi-Fi signals can be controllably enhanced at arbitrarily prescribed locations assisted with programmable metasurface. To that end, we, for the first time, propose an efficient optimization algorithm for the scenario of Wi-Fi signals enhancements using programmable metasurface, in which the complex amplitude patterns of Wi-Fi field bounced off metasurface have been carefully reengineered. Then, we fabricate a large-scale programmable metasurface working at around 2.4 GHz to demonstrate the developed strategy. Theoretical and experimental results show that Wi-Fi signals have been successfully enhanced at multiple locations in a controllable and flexible manner. Moreover, an increase by a factor of 23.5 dB in the received intensity level of commodity Wi-Fi signals, has been achieved when the programmable metasurface is written with optimized coding sequences.

The remaining of this paper is organized as follows. In Section 2, we will firstly present a large-scale phase-binary programmable coding metasurface working at around 2.4 GHz which is utilized to manipulate Wi-Fi signals. Afterwards, we will elaborate on the proposed efficient optimization algorithm to achieve the optimal coding sequences of programmable metasurface such that the desirable spatial energy distribution of ambi-

ent Wi-Fi signals can be obtained. Later on, selected experimental results are provided to demonstrate the performance of the proposed methodology in controlling the spatial energy of ambient Wi-Fi signals. These experiments are performed using an IEEE 802.11b commercial wireless device (off-the-shelf) working at the 7th channel (2.442 GHz) with bandwidth of 20 MHz. Finally, some concluding remarks are summarized in Section 5.

2 Design of Tunable Metasurface

2.1 Design of electronically-controllable unit cells

The unit cell structure of the programmable metasurface utilized to manipulate Wi-Fi signals is illustrated in Fig. 1(a), which is composed of a 37.2 mm length of square patch and a metal ground layer spaced by the 1.5 mm thickness of F_4BM substrate with dielectric constant of 2.55 and loss tangent of 0.0015. A 90°-bending strip, 0.8 mm in width and 14.6 mm in length, is connected to the ground plane through a metal via. A PIN diode with low insertion loss (≤0.2 dB) and high isolation (≥13 dB) in 2.4 GHz Wi-Fi band has been introduced at the gap between the square path and the 90°-bending strip. The 0.7 mm thickness of substrate (FR-4) has been mounted below the ground plane in order to feed the PIN diode with external DC voltage. To achieve good isolation between the RF and DC signals, we introduce an inductor with inductance of L=33 nH whose self-resonance frequency is higher than 3.5 GHz.

The unit cell has been simulated using CST Microwave Studio, in which the PIN diode is modelled as an equivalent lumped circuit, as used in Ref. [26]. Simulated and measured results of the unit cell are plotted in Fig. 1(b), which are in well agreements with each other. The red lines denote amplitude responses of unit cell, while the blue one denote phase responses of unit cell. It can be readily observed that the simulated reflection amplitudes are larger than 0.8, and the frequency bandwidth of phase difference between 180°±20° is from 2.401 GHz to 2.456 GHz, covering 8 channels of commodity Wi-Fi Frequency bands. Although the proposed electronically-controllable unit cell does not cover all the channels at 2.4 GHz Wi-Fi frequency band, slotting technology can be used to significantly improve the working frequency band[27,28].

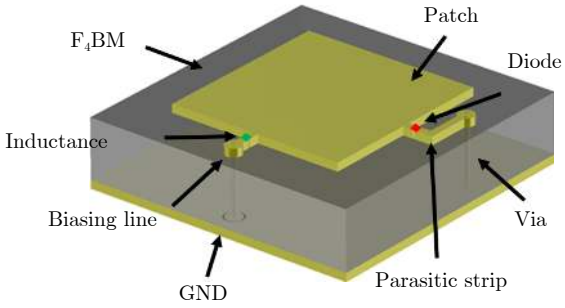

(a) Perspective view of the unit cell

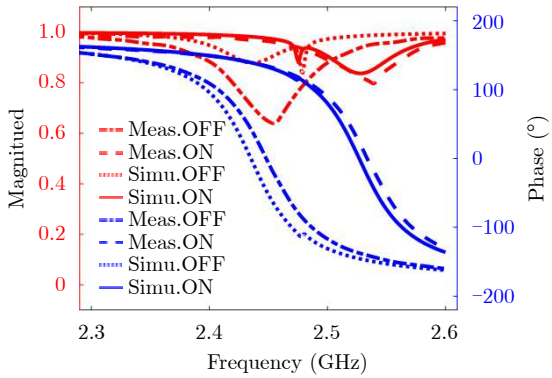

(b) Simulated and experimental EM responses of the unit cell

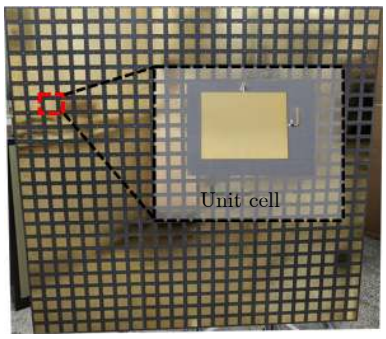

(c) The fabricated metasurface prototype

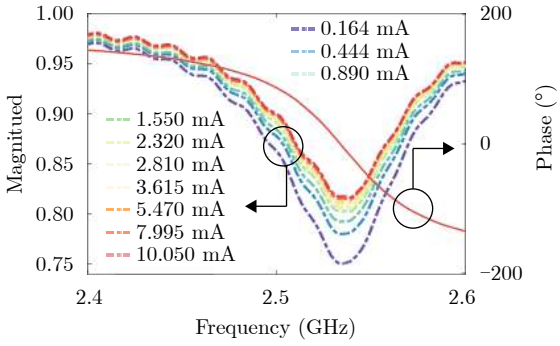

(d) The EM responses of the unit cell at ON status with varying drive current

Fig. 1 Description of programmable metasurface and EM responses

2.2 Fabrication of large-scale tunable metasurface

A 1.296 m length of metasurface composed of 24×24 independently controlled unit cells has been fabricated using standard printed circuit board technology, as shown in Fig. 1(c). The whole metasurface has been divided into 3×3 subpanels, and each subpanel is equipped with 8 bit shift registers to respectively control eight PIN diodes which are connected in series. A dedicated FPGA-based micro board with the clock rate of 50 MHz has been designed to distribute all commands to all PIN diodes, with the ideal switching time of 10 μs.

It is worth mentioning that there are two critical issues in designing a large-scale programmable coding metasurface. The first is about the insufficient driving capability of shift registers chips subject to the limited energy expenditure available, which can be solved by introducing an external biasing voltage for each PIN diode by a BJT, as used in Refs. [1,29]. The second issue is about the limited energy budget available. To reduce as much power consumption as possible, for each PIN diode, the relationship between the power consumption and EM response characteristic of the meta-atom at ON status has been investigated using so-called waveguide method[30] in Fig. 1(d). It can be drawn that the EM responses of the designed meta-atom at ON status remains almost unchanged as the drive current of PIN diode is larger than 1.550 mA. Based on above observations, for each PIN diode, we use a 680 Ω current limiting resistance to restrict its driving current to 3.38 mA at 0.85 V. Then, the total power dissipated by all PIN diodes at ON status is about 1.6 W, which is much lower than that are reported in[29,31].

3 Optimization Algorithm of Coding Sequence of Metasurface

In order to tailor ambient Wi-Fi signals using large-scale metasurface in a desirable way, one critical issue is to find the matching coding sequences of the programmable metasurface. Although many efforts in published works have been made to optimize the control sequences of metasurfaces, they only aim at re-engineering the spatial amplitude patterns of scattering field or radiation field of metasurfaces, whether in the far-field region[1,23–25,31–32] or near-field region[6–12,33]. Being different, we elaborate on the redesign of spatial complex amplitude patterns of Wi-Fi field bounced off the metasurface, which means that the optimization goal of the proposed algorithm is not only to maximize the amplitude of Wi-Fi field scattered from metasurface at prescribed locations, but also to make the focused scattering wave in-phase with the direct wave from Wi-Fi router at given locations. We first establish an effective EM scattering model of metasurafce which is much faster than using the CST microwave studio package under same computation configuration. Then, we propose a Complex Weighted Gerchberg-Saxton (CWGS) algorithm based on the EM scattering model to redesign complex amplitude patterns of Wi-Fi field bounced off the metasurface. By adopting this kind of strategy, significant enhancements of Wi-Fi signals at prescribed locations can be successfully achieved.

3.1 EM scattering model of binary-phase metasurface

To illustrate our methodology, we consider the scenario where the programmable coding metasurface, composed of $N\times M$ phase-binary unit cells, is exposed to the illumination of Wi-Fi signals emitted from a wireless device. To achieve the spatial energy distribution of Wi-Fi signals with enough accuracy when the programmable coding metasurface exists, we made two-aspect efforts as follows. First, the scattering field of unit cells has been modeled in terms of the well-known Huygens' principle, by which more realistic EM responses of the unit cells can be considered. Second, the total scattering Wi-Fi field from the whole coding metasurface aperture has be synthesized according to the superposition principle.

First, we focus on the prediction of EM responses of unit cells. In light of the well-known Huygens' principle, we know that the EM responses of meta-atoms can be accurately obtained once its induced equivalent current is obtained. Taking this fact into account, we start by evenly dividing the meta atom into $P\times Q$ grids

with subwavelength scale, then the induced current over each grid is approximated to be uniform. The relationship between the scattering field $\boldsymbol{E}_{\mathrm{a}}$ of each unit cell at observation position $\boldsymbol{r}$ and its induced equivalent current $\boldsymbol{J}$ can be represented as $\boldsymbol{E}_{\mathrm{a}}=\boldsymbol{A}\boldsymbol{J}$, in which

$$\boldsymbol{A}=i\omega\mu\Delta\begin{bmatrix} G^{x,x}_{\boldsymbol{r},\boldsymbol{r}'_{11}} & G^{x,y}_{\boldsymbol{r},\boldsymbol{r}'_{11}} & G^{x,x}_{\boldsymbol{r},\boldsymbol{r}'_{12}} & G^{x,y}_{\boldsymbol{r},\boldsymbol{r}'_{12}} & \cdots & G^{x,x}_{\boldsymbol{r},\boldsymbol{r}'_{PQ}} & G^{x,y}_{\boldsymbol{r},\boldsymbol{r}'_{PQ}} \\ G^{y,x}_{\boldsymbol{r},\boldsymbol{r}'_{11}} & G^{y,y}_{\boldsymbol{r},\boldsymbol{r}'_{11}} & G^{y,x}_{\boldsymbol{r},\boldsymbol{r}'_{12}} & G^{y,y}_{\boldsymbol{r},\boldsymbol{r}'_{12}} & & G^{y,x}_{\boldsymbol{r},\boldsymbol{r}'_{PQ}} & G^{y,y}_{\boldsymbol{r},\boldsymbol{r}'_{PQ}} \end{bmatrix} \tag{1}$$

$$\boldsymbol{J}=\begin{bmatrix} J^{x}_{\boldsymbol{r}'_{11}} & J^{y}_{\boldsymbol{r}'_{11}} & J^{x}_{\boldsymbol{r}'_{12}} & J^{y}_{\boldsymbol{r}'_{12}} & \cdots & J^{x}_{\boldsymbol{r}'_{PQ}} & J^{y}_{\boldsymbol{r}'_{PQ}} \end{bmatrix}^{\mathrm{T}} \tag{2}$$

Here, Δ represents the area of each grid, $\boldsymbol{r}'$ goes over the central coordinate of all divided grids, the entries of $\boldsymbol{A}$ comes from the Dyadic Green's function. Then, a model that a unit cell either at "ON" or "OFF" status illuminated by a plane wave is calculated through numerical simulation, and the resultant scattering field $\boldsymbol{E}_{\mathrm{a}}$ is collected at a distance far enough from the unit cell. Now, the least-square method can be used to retrieve the induced equivalent current $\boldsymbol{J}$, namely,

$$\boldsymbol{J}=\left(\boldsymbol{A}'\boldsymbol{A}+\gamma\boldsymbol{I}\right)^{+}\boldsymbol{A}'\boldsymbol{E}_{\mathrm{a}} \tag{3}$$

where γ denotes an artificial regularization parameter, $\boldsymbol{I}$ means the unit matrix, and + presents the matrix pseudo inverse. In our specific implementations, the surface of the unit cell is uniformly divided to 10×10 square grids with area of $0.044\lambda\times0.044\lambda$, and the scattering field $\boldsymbol{E}_{\mathrm{a}}$ is obtained in an observation plane 0.5λ away from the meta-atom which is illuminated by a plane wave with intensity of 1 V/m. The equivalent induced current of the meta-atom at 2.442 GHz can be calculated according to Eq. (3), where $\gamma=10^{10}$ is used.

Second, we synthesize the total EM field induced from the whole programmable metasurface illuminated by Wi-Fi signals in terms of the superposition principle. For simplify, a single Wi-Fi router with the same polarization of unit cell, is placed to obliquely illuminate programmable metasurface at an angle of –20°. By treating Wi-Fi router as a dipole antenna, its far-field radiation field can be approximated as following, *i.e.*,

$$E^{\mathrm{in}}\left(\boldsymbol{r}_{\mathrm{f}}\right)=C_0\sin^{q_{\mathrm{f}}}\varphi_{\boldsymbol{r}_{\mathrm{f}}}\frac{\exp\left(-\mathrm{j}k_0\left|\boldsymbol{r}_{\mathrm{f}}\right|\right)}{\left|\boldsymbol{r}_{\mathrm{f}}\right|} \tag{4}$$

where C_0 is an energy coefficient, q_{f} is the radiation pattern factor of Wi-Fi router which is set to be 1 in our simulation. And $\varphi_{\boldsymbol{r}_{\mathrm{f}}}$ denotes the angle between observation position $\boldsymbol{r}_{\mathrm{f}}$ in the coordinate system centered at Wi-Fi source and x axis. As a consequence, the co-polarized electrical field scattered from the whole metasurface aperture illuminated by a Wi-Fi router can be expressed as following, *i.e.*,

$$\boldsymbol{E}_{\mathrm{s}}=\sum_{n_x=1}^{N}\sum_{n_y=1}^{M}\boldsymbol{A}(\boldsymbol{r},\boldsymbol{r}_{n_x,n_y})\boldsymbol{\Lambda}_{n_x,n_y}\boldsymbol{J}^{\mathrm{ON/OFF}}_{n_x,n_y} \tag{5}$$

Herein, $\boldsymbol{\Lambda}_{n_x,n_y}=E^{\mathrm{in}}\left(\boldsymbol{r}_{n_x,n_y}\right)\boldsymbol{I}$, $\boldsymbol{I}$ is a diagnal square matrix with length of $2\times P\times Q$, $E^{\mathrm{in}}\left(\boldsymbol{r}_{n_x,n_y}\right)$ and $\boldsymbol{J}^{\mathrm{ON/OFF}}_{n_x,n_y}$ denote the incident Wi-Fi wave and the induced current on the $(n_x,n_y)^{\mathrm{th}}$ meta atom along x and y directions, respectively, and the double summation involved in Eq. (5) is performed over all unit cells of metasurface. Here, we would like to say that the EM scattering model outlined above only costs a few minutes, which is much faster than using the CST microwave studio package under the same computation configuration in a personal computer. Also, the EM scattering model can be implemented not only in far field region but also in near filed region since the Green's function in the model has not been approximated.

3.2 Complex weighted G-S algorithm for finding the optimal coding sequence of metasurface

Now, to the best of our knowledge, a CWGS algorithm based on aforementioned EM scattering model, was proposed for the first time to find the optimal coding sequences of the metasurface, particularly for the scenario of Wi-Fi signals enhancements at desired locations. On one hand the CWGS algorithm is performed to focus the Wi-Fi field scattered from metasurface at given locations, on the other hand it is aimed at making the direct wave from Wi-Fi router in-phase with the focused scattering wave bounced off the metasurface. Therefore, constructive interference of Wi-Fi

signals at prescribed locations can be obtained. A critical parameter in the proposed algorithm is the complex weight χ_m, which is used to adjust the complex amplitude patterns of scattering field of metasurface at the mth desired location $\boldsymbol{r}_m$. The iteration process of the complex-valued weight has been presented as follows:

$$\text{0th step} \quad \chi_m^{(0)} = \beta_m \exp\left(-\mathrm{j}k_0\left|\boldsymbol{r}_m - \boldsymbol{r}_\mathrm{s}\right|\right) \tag{6}$$

$$k\text{th step} \quad \chi_m^{(k)} = \frac{\chi_m^{(0)}}{\sum\limits_m \left|\chi_m^{(0)}\right|} \cdot \frac{\sum\limits_m \left|E_\mathrm{s}^{(k-1)}\left(\boldsymbol{r}_m\right)\right|}{E_\mathrm{s}^{(k-1)}\left(\boldsymbol{r}_m\right)} \cdot \left|\chi_m^{(k-1)}\right| \tag{7}$$

where $\boldsymbol{r}_\mathrm{s}$ denotes the location of Wi-Fi router, β_m denotes the amplitude weight of scattering field at location $\boldsymbol{r}_m$, and k_0 denotes the wavenumber in vacuum. It should be clarified that the phase weight $\varphi_m = -k_0\left|\boldsymbol{r}_m - \boldsymbol{r}_\mathrm{s}\right|$ is utilized to make the focused scattering wave from the metasurface in-phase with the direct wave from Wi-Fi router at identical location $\boldsymbol{r}_m$. And β_m can be utilized to adjust the amplitude weight ratio of Wi-Fi signals at different locations. Here, we set every β_m equal 1 at all desired locations for simplicity.

Algorithm. The Complex Weighted G-S algorithm.

Initial random coding sequence

$k = 0, \boldsymbol{\chi}^{(0)} = \left[\begin{array}{ccccc} \chi_1^{(0)} & \cdots & \chi_m^{(0)} & \cdots & \chi_M^{(0)} \end{array}\right]^\mathrm{T}$

$\tilde{\boldsymbol{E}}_\mathrm{s}^{(0)} = \tilde{\boldsymbol{A}}\tilde{\boldsymbol{\Lambda}}\tilde{\boldsymbol{J}}^{(0)}$

WHILE NOT convergence

· Update $\boldsymbol{\chi}^{(k)}$ from Eq. (7)

· $\widehat{\boldsymbol{E}}_\mathrm{s}^{(k)} = \mathrm{diag}\left(\boldsymbol{\chi}^{(k)}\right)\exp\left[\mathrm{jangle}\left(\tilde{\boldsymbol{E}}_\mathrm{s}^{(k)}\right)\right]$

· $\widehat{\boldsymbol{J}}^{(k+1)} = \left[\tilde{\boldsymbol{A}}\tilde{\boldsymbol{\Lambda}}\right]^\mathbf{H}\widehat{\boldsymbol{E}}_\mathrm{s}^{(k)}$

· $\tilde{\boldsymbol{J}}_{(n_x,n_y)}^{(k+1)} = \begin{cases} \boldsymbol{J}^\mathrm{ON}, \text{if angle}\left[\widehat{\boldsymbol{J}}_{(n_x,n_y)}^{(k+1)}\right] \in \theta_1 \\ \boldsymbol{J}^\mathrm{OFF}, \text{if angle}\left[\widehat{\boldsymbol{J}}_{(n_x,n_y)}^{(k+1)}\right] \in \theta_2 \end{cases}$,

$\theta_1 \cup \theta_2 = [0, 2\pi]$

· $\tilde{\boldsymbol{E}}_\mathrm{s}^{(k+1)} = \tilde{\boldsymbol{A}}\tilde{\boldsymbol{\Lambda}}\tilde{\boldsymbol{J}}^{(k+1)}$

· $k \Leftarrow k+1$

END WHILE

Additionally, Eq. (5) can be rewritten in compact form as $\tilde{\boldsymbol{E}}_\mathrm{s}^{(k)} = \tilde{\boldsymbol{A}}\tilde{\boldsymbol{\Lambda}}\tilde{\boldsymbol{J}}^{(k)}$ for numerical implementation. Then the proposed algorithm is summarized in *Algorithm*. Apparently, such solution strategy behaves in an iterative way. After several seconds, the stable convergence can be achieved. It is stressed that different phase range θ_1 and θ_2 in the algorithm will lead to different optimization results when adjusting coding sequence according to the phase of induced current of unit cells. Therefore, it is necessary to scan the phase range to obtain better results.

Fig. 2 shows several numerical results of the proposed CWGS algorithm in three cases, *i.e.*, "Monofocal", "Bifocal" and "Trifocal", in which the algorithm has been adopted not only to focus the intensity of scattering field from the metasurface at given locations but also adjust the phase of scattering field at identical positions according to pre-specified phase. Fig. 2(a) and Fig. 2(b) respectively presents the iteration process of the amplitude and phase of scattering field from metasurface at same locations when the developed CWGS algorithm is applied. In the case of "Monofocal", the scattering field intensity has been remarkably improved and the field phase at identical location has been readjusted to a preferred phase 90°. Similarly, the complex-valued scattering field from metasurface at multiple locations, corresponding to the case of "Bifocal" and "Trifocal", has been successfully focused with various desired phases.

3.3 Near-field scanning of tunable coding metasurface

In this subsection, a set of simulation and experimental results of spatial field distribution have been provided to illustrate the proposed method of enhancing Wi-Fi signals at desired locations. The measurement setup is shown in Fig. 3, in which Wi-Fi signals are mimicked by a Vector Network Analyzer (VNA) and near-field scanning technique is utilized to measure the field distribution. The VNA is connected with a Wi-Fi transmitting antenna and an open-ended waveguide probe to scan the near-field distribution by measuring the transmission coefficients S_{12} in an observation plane. Additionally, the Wi-Fi transmitting antenna is located at the position of (0, –0.291 m, 0.8 m). The scanning area is a 0.945 m× 0.945 m square with sampling space of 0.0315 m.

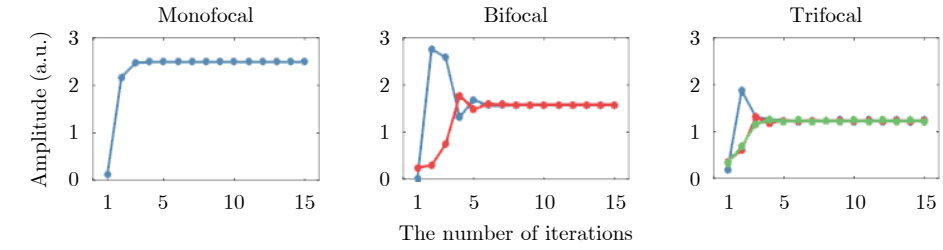

(a) The iteration process of scattering field's amplitude

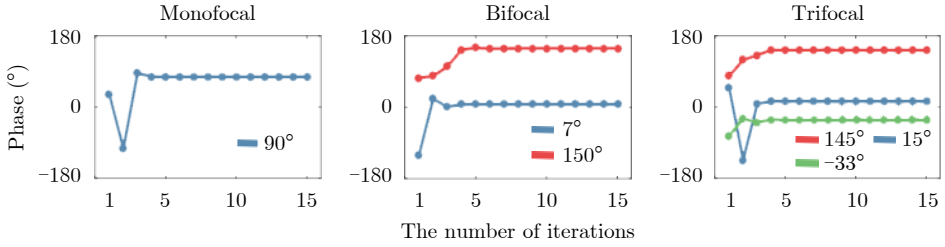

(b) The iteration process of scattering field's phase

Fig. 2 The iteration process of amplitude and phase of scattering field bounced off metasurface at given locations for three cases when the developed CWGS algorithm is applied

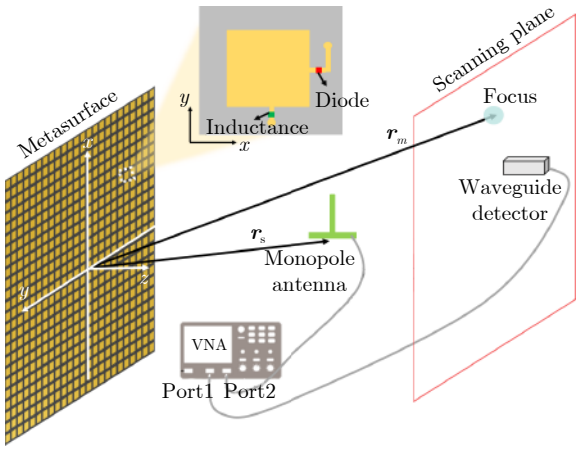

Fig. 3 The measurement setup of near-field scanning

Here, we consider six coding sequences of programmable metasurface, as shown in the top row of Fig. 4. Accordingly, the spatial distribution of mimicked Wi-Fi signals at three observation planes in the distance of z=0.984 m, 1.257 m, and 1.531 m away from the programmable coding metasurface, have been reported in the second to fourth rows of Fig. 4, respectively. All the electrical field distributions have been normalized by their own maximums. For comparison, the experimental results at the observation plane of z=1.531 m are also provided in the bottom row of Fig. 4. It should be pointed out that the coding sequences have been particularly optimized at the plane z=0.984 m, which means that the focusing performance of the metasurface at z=0.984 m will be better than other planes. As expected, the predicted intensity allocations for all coding sequences are gradually becoming distorted with the growth of observation plane distance. Better performance of intensity allocation at different planes will be achieved if adaptive optimizations are performed according to the distance. The experimental results at z=1.531 m plane shows well agreement with the theoretical results at the identical plane and validate the effectiveness of the proposed method. There are some discrepancies between the experimental results and numerical predictions probably due to the complicated environment of an ordinary office room.

Then, the important efficiency analysis has also been conducted in this subsection. Here, we define the focus efficiency as the ratio of P_{f} (the power of the focus area in the designated observation plane) and P_{t} (the total power in the designated observation plane). Two kinds of focus efficiency corresponding to the aforementioned six simulated cases observed in z=0.984 m plane have been considered, in which the P_{f} is obtained within two kinds of focus regions where the normalized field intensity is larger than –3 dB and –6 dB, respectively. The results are summarized in Tab. 1.

4 Experiments Against Commodity Wi-Fi Signals

In this section, several experimental results of

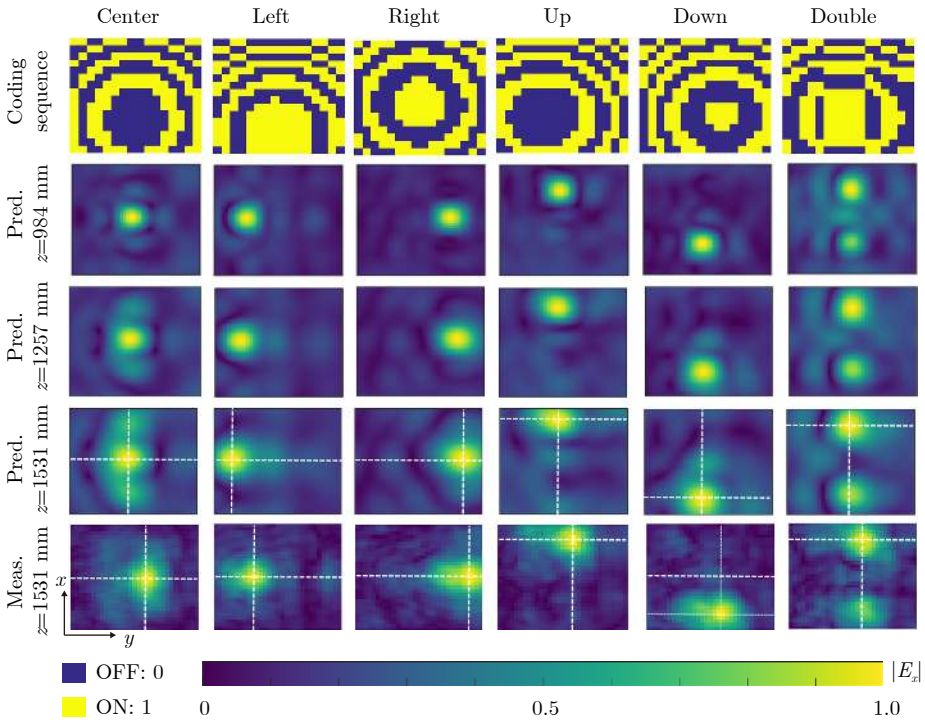

Fig. 4 Results comparison between prediction and measurement

The first row are the coding sequences. The second to fourth rows are the normalized spatial intensity distributions predicted respectively at z=0.984 m, z=1.257 m, and z=1.531 m using the proposed method. The fifth row are the measured normalized spatial intensity distributions at z=1.531 m using the near-field scanning technology

Tab. 1 The focus efficiency for six different cases

Cases (dB)	Center (%)	Left (%)	Right (%)	Up (%)	Down (%)	Double (%)
–3	25.36	30.73	40.24	28.51	35.27	21.27
–6	37.42	45.19	59.32	41.81	51.96	38.65

enhancing commodity Wi-Fi signals, transmitted by an off-the-shelf wireless device, are provided to further demonstrate the proposed strategy, along with a potential real-world application in achieving complicated energy allocation of Wi-Fi signals.

4.1 Enhancement of commodity Wi-Fi signals at desired locations

With reference to Fig. 5, a Wi-Fi router working at the 7th operational channel, *i.e.*, 2.431～2.453 GHz, is randomly placed somewhere in front of the programmable metasurface. And three commercial parabolic antennas, respectively connected with three ports of an oscilloscope, are deployed at different locations marked in Fig. 5 to acquire the commodity Wi-Fi signals. In the first set of experimental investigations, we examine the controllable feature of the proposed strategy by

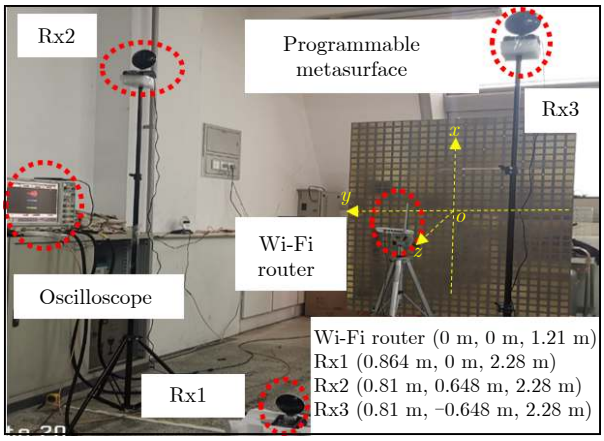

Fig. 5 Practical experimental setup using the commercial Wi-Fi device

focusing commodity Wi-Fi signals at a single position located at Rx2. Six different coding sequences, shown in Fig. 6(a), are respectively written in the programmable metasurface. Here, we denote the "Full dark" by setting all PIN diodes of metasurface to be "OFF" status, while the "Full bright" by setting all PIN diodes to be "ON" status. Accordingly, the time-domain Wi-Fi signals within the duration of 2 μs for six cases are measured by the oscilloscope. In order to

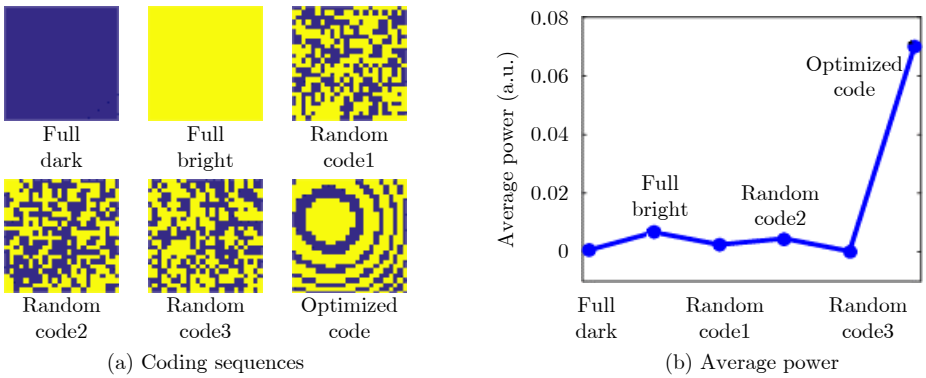

Fig. 6 Measured results of focusing commodity Wi-Fi signals at a single position located at Rx2

clearly present the great performance of the proposed strategy, the average power of measured Wi-Fi signals in six cases are calculated and plotted in Fig. 6(b). It is obvious that the average power of received Wi-Fi signals vary significantly with the choices of coding sequences, and only when the programmable metasurafce is written with the optimized coding sequence, the maximum average power can be obtained, with an increase in signal power level by a factor of 10.43, compared with the case of "full bright".

Another set of experimental demonstrations has also been performed to examine the flexible feature of the proposed strategy by optimizing the coding sequence of metasurface from enhancing commodity Wi-Fi signals at single position to multiple positions. We have considered three scenarios, *i.e.*, "Monofocal", "Bifocal" and "Trifocal". Here, "Monofocal" denotes enhancing Wi-Fi signals at single location. "Bifocal" denotes simultaneously enhancing Wi-Fi signals at double locations. And, "Trifocal" denotes simultaneously enhancing Wi-Fi signals at all positions marked in Fig. 7. The measured time-domain waveforms and frequency spectrums of received signals are respectively provided in Fig. 7(a) and Fig. 7(b) for six selected cases. Apparently, experimental results show that flexible control of commodity Wi-Fi signals with remarkable enhancements at multiple positions has been successfully realized, with the help of our developed approach and programmable metasurface.

Besides, we have conducted several control experiments that commodity Wi-Fi signals are measured at identical locations without using programmable metasurface. Compared with the measured results in control experiments, increases by a factor of 22.6 dB and 23.5 dB in the intensity level of measured Wi-Fi signals at Rx1 and Rx3 in Fig. 7 have been respectively achieved empowered by programmable metasurface, which further demonstrates the great performance of our developed approach.

4.2 Promising applications of controllable enhancement of Wi-Fi signals using programmable metasurface

In this subsection, we would like to say that instead of point-like energy enhancements of Wi-Fi signals, other more complicated energy allocation of Wi-Fi signals also can be achieved in principle by adopting the proposed strategy. In order to show this, another set of numerical simulations results are provided in Fig. 8. Here, we consider such a scenario in which the metasurface is mounted on the ceiling inside a house. In order to avoid complex modeling of indoor scene, we assume that initial Wi-Fi field in observation plane and the one illuminated on programmable metasurface are both randomly distributed in our simulation, as shown in Fig. 8(c). Then the indoor Wi-Fi signals are controlled to be concentrated in some desired areas simultaneously such as two bedrooms and a table in the living room, as shown in Fig. 8(d), by properly re-engineering the coding sequences.

Finally, we would like to clarify the superiority of our developed method by comparing with the existing works dealing with EM waves manipulation using metasurface. The comparison has been summarized in Tab. 2. It is clear that our

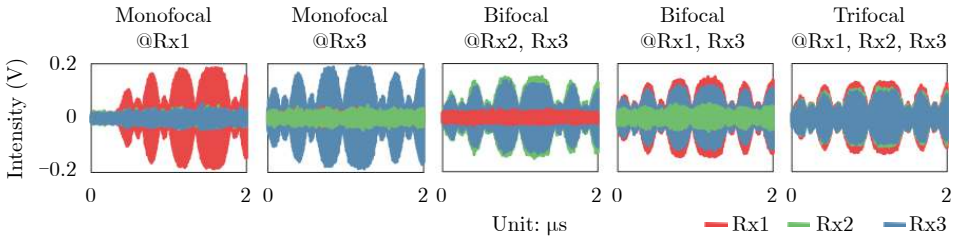

(a) Measured Wi-Fi waveforms in time-domain

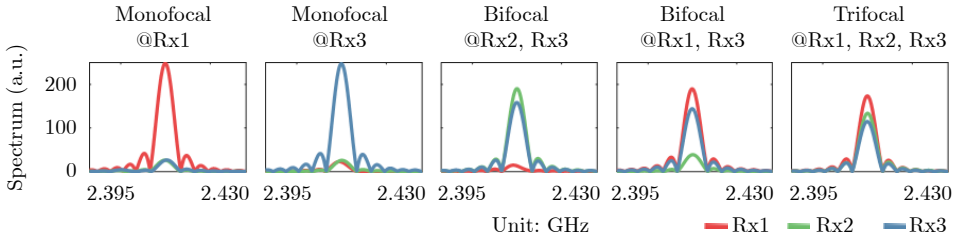

(b) Calculated spectrums in frequency-domain

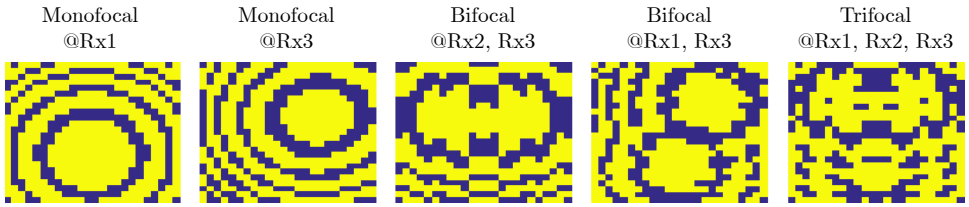

(c) The corresponding coding sequences

Fig. 7 Experimental results for flexible and dynamic enhancements of commodity Wi-Fi signals at multiple locations

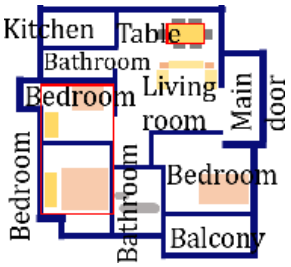

(a) Floor plan

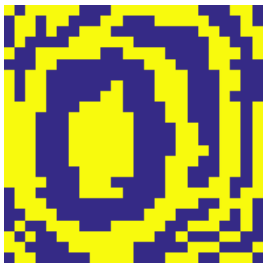

(b) Coding sequences

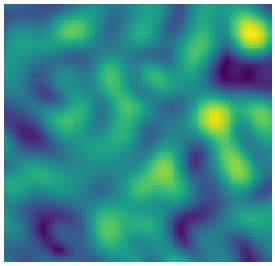

(c) Before adjusting

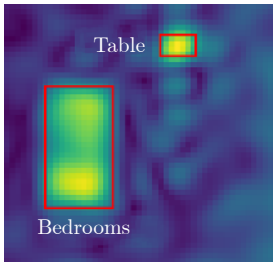

(d) After adjusting

Fig. 8 The simulation of complicated energy allocation of Wi-Fi signals in a typical indoor environment

proposed strategy, allocating the energy distribution of Wi-Fi signals, works in a passive manner which means no dedicated source is required. Besides, our developed method makes full use of EM waves by manipulating the complex amplitude patterns of scattering field from metasurface, which enhances the ability to control EM waves.

5 Conclusions

In this work, we have demonstrated the idea of tailoring commodity Wi-Fi signals using programmable metasurface by theoretical and experimental investigations. An efficient optimization algorithm based on a fast EM scattering model, was developed for the first time to manipulating both the amplitude and phase information of scattering Wi-Fi field bounced off metausrface. By adopting the proposed algorithm, we have realized ambient Wi-Fi signals enhancements at desired locations in a dynamic and controllable manner, assisted with a large-scale programmable metasurface working at around 2.4 GHz. Both the simulated and measured results approve that our strategy works well in flexible control of commodity Wi-Fi signals. An increase by a factor of 23.5 dB in the intensity level of Wi-Fi signals, has been achieved compared with the case without programmable metausurface.

Since the programmable metasurface is capable of extremely fast switching time, the spa-

Tab. 2 Comparing with the existing works dealing with EM waves manipulation using metasurface

Ref.	f_0 (GHz)	Source type	Working mode of metasurface	Optimization goal of algorithm	Working region	The shape of energy allocation	Reconfig-urability	Maximum focusing efficiency
[6]	6.9	Dedicated source	Active	Field's amplitude pattern	Near-field	Point-like	YES	–
[7]	10	Dedicated source	Active	Field's amplitude pattern	Near-field	Point-like	NO	57.8%
[8]	5.75	Dedicated source	Active	Field's amplitude pattern	Near-field	Point-like	YES	–
[9]	10	Dedicated source	Active	Field's amplitude pattern	Near-field	Point-like	YES	–
[10]	20	Dedicated source	Active	Field's amplitude pattern	Near-field	Point-like	NO	52.3%
[11]	10	Dedicated source	Active	Field's amplitude pattern	Near-field	Point-like	NO	–
[12]	5.8	Dedicated source	Active	Field's amplitude pattern	Near-field	Point-like	NO	–
[31]	14.3	Dedicated source	Active	Field's amplitude pattern	Far-field	Single beam	YES	–
[23]	5.8	Dedicated source	Active	Field's amplitude pattern	Near-field	Point-like	NO	–
[24]	2.3	Dedicated source	Active	Field's amplitude pattern	Far-field	Single beam	YES	–
[25]	10	Dedicated source	Active	Field's amplitude pattern	Far-field	Single beam	YES	
Proposed	2.4	Commodity wireless device	Passive	Field's complex amplitude pattern	Not limited	Not limited	YES	59.32%

tial Wi-Fi signals can be rapidly manipulated by control commands sent from master computer through a real-time communication. Therefore, it could be faithful that our proposed strategy will pave a promising way for building an intelligent Wi-Fi environment and promote the development of future wireless communications and so on.

References

[1] YANG Huanhuan, CAO Xiangyu, YANG Fan, *et al.* A programmable metasurface with dynamic polarization, scattering and focusing control[J]. *Scientific Reports*, 2016, 6: 35692. doi: 10.1038/srep35692.

[2] LI Lianlin, CUI Tiejun, JI Wei, *et al.* Electromagnetic reprogrammable coding-metasurface holograms[J]. *Nature Communications*, 2017, 8(1): 197. doi: 10.1038/s41467-017-00164-9.

[3] LAROUCHE S, TSAI Y J, TYLER T, *et al.* Infrared metamaterial phase holograms[J]. *Nature Materials*, 2012, 11(5): 450–454. doi: 10.1038/nmat3278.

[4] LI Lianlin, RUAN Hengxin, LIU Che, *et al.* Machine-learning reprogrammable metasurface imager[J]. *Nature Communications*, 2019, 10(1): 1082. doi: 10.1038/s41467-019-09103-2.

[5] LI Lianlin and CUI Tiejun. Information metamaterials – from effective media to real-time information processing systems[J]. *Nanophotonics*, 2019, 8(5): 703–724. doi: 10.1515/nanoph-2019-0006.

[6] CHEN Ke, FENG Yijun, MONTICONE F, *et al.* A reconfigurable active huygens' metalens[J]. *Advanced Materials*, 2017, 29(17): 1606422. doi: 10.1002/adma.201606422.

[7] WANG Yue, GUAN Chunsheng, DING Xumin, *et al.* Multi-focus hologram utilizing Pancharatnam-Berry phase elements based metamirror[J]. *Optics Letters*, 2019, 44(9): 2189–2192. doi: 10.1364/OL.44.002189.

[8] WANG Zehao, LIAO Dashuang, ZHANG Ting, *et al.* Metasurface-based focus-tunable mirror[J]. *Optics Express*, 2019, 27(21): 30332–30339. doi: 10.1364/OE.27.030332.

[9] ZHANG Kuang, YUAN Yueyi, DING Xumin, *et al.* High-efficiency metalenses with switchable functionalities in microwave region[J]. *ACS Applied Materials & Interfaces*, 2019, 11(31): 28423–28430.

[10] GOWDA V R, IMANI M F, SLEASMAN T, *et al.* Focusing microwaves in the fresnel zone with a cavity-backed holographic metasurface[J]. *IEEE Access*, 2018, 6: 12815–12824. doi: 10.1109/ACCESS.2018.2802379.

[11] ZHANG Pei, LI Long, ZHANG Xuanming, *et al.* Design, measurement and analysis of near-field focusing reflective metasurface for dual-polarization and multi-focus wireless power transfer[J]. *IEEE Access*, 2019, 7: 110387–110399. doi: 10.1109/ACCESS.2019.2934135.

[12] YU Shixing, LIU Haixia, and LI Long. Design of near-field focused metasurface for high-efficient wireless power transfer with multifocus characteristics[J]. *IEEE Transactions on Industrial Electronics*, 2019, 66(5): 3993–4002. doi: 10.1109/TIE.2018.2815991.

[13] ZHAO Jie, YANG Xi, DAI Junyan, *et al.* Programmable time-domain digital-coding metasurface for non-linear harmonic manipulation and new wireless communication

systems[J]. *National Science Review*, 2019, 6(2): 231–238. doi: 10.1093/nsr/nwy135.

[14] ZHANG Xu, GRAJAL J, VAZQUEZ-ROY J L, *et al*. Two-dimensional MoS_2-enabled flexible rectenna for Wi-Fi-band wireless energy harvesting[J]. *Nature*, 2019, 566(7744): 368–372. doi: 10.1038/s41586-019-0892-1.

[15] WANG Guanhua, ZOU Yongpan, ZHOU Zimu, *et al*. We can hear you with Wi-Fi![J]. *IEEE Transactions on Mobile Computing*, 2016, 15(11): 2907–2920. doi: 10.1109/TMC.2016.2517630.

[16] ALI K, LIU A X, WANG Wei, *et al*. Keystroke recognition using WiFi signals[C]. The 21st Annual International Conference on Mobile Computing and Networking, Paris, France, 2015: 90–102.

[17] WU Xuangou, CHU Zhaobin, YANG Panlong, *et al*. TW-see: Human activity recognition through the wall with commodity Wi-Fi devices[J]. *IEEE Transactions on Vehicular Technology*, 2019, 68(1): 306–319. doi: 10.1109/TVT.2018.2878754.

[18] XU Qinyi, CHEN Yan, WANG Beibei, *et al*. Radio biometrics: Human recognition through a wall[J]. *IEEE Transactions on Information Forensics and Security*, 2017, 12(5): 1141–1155. doi: 10.1109/TIFS.2016.2647224.

[19] HOLL P M and REINHARD F. Holography of Wi-Fi radiation[J]. *Physical Review Letters*, 2017, 118(18): 183901. doi: 10.1103/PhysRevLett.118.183901.

[20] ZHONG Wei, HE W K, WANG Longgang, *et al*. Through-the-wall imaging using Wi-Fi signals[C]. The 2018 12th International Symposium on Antennas, Propagation and EM Theory, Hangzhou, China, 2018: 1–3.

[21] LI Lianlin, SHUANG Ya, MA Qian, *et al*. Intelligent metasurface imager and recognizer[J]. *Light*: *Science & Applications*, 2019, 8: 97.

[22] TANG Wankai, DAI Junyan, CHEN Mingzheng, *et al*. Programmable metasurface-based RF chain-free 8PSK wireless transmitter[J]. *Electronics Letters*, 2019, 55(7): 417–420. doi: 10.1049/el.2019.0400.

[23] GOWDA V R, YURDUSEVEN O, LIPWORTH G, *et al*. Wireless power transfer in the radiative near field[J]. *IEEE Antennas and Wireless Propagation Letters*, 2016, 15: 1865–1868. doi: 10.1109/LAWP.2016.2542138.

[24] DAI Linglong, WANG Bichai, WANG Min, *et al*. Reconfigurable intelligent surface-based wireless communications: Antenna design, prototyping, and experimental results[J]. *IEEE Access*, 2020, 8: 45913–45923. doi: 10.1109/ACCESS.2020.2977772.

[25] RATNI B, DE LUSTRAC A, PIAU G P, *et al*. Reconfigurable meta-mirror for wavefronts control: Applications to microwave antennas[J]. *Optics Express*, 2018, 26(3): 2613–2624. doi: 10.1364/OE.26.002613.

[26] XU Hexiu, SUN Shulin, TANG Shiwei, *et al*. Dynamical control on helicity of electromagnetic waves by tunable metasurfaces[J]. *Scientific Reports*, 2016, 6: 27503. doi: 10.1038/srep27503.

[27] WANG Di, YIN Lizheng, HUANG Tiejun, *et al*. Design of a 1 bit broadband space-time-coding digital metasurface element[J]. *IEEE Antennas and Wireless Propagation Letters*, 2020, 19(4): 611–615. doi: 10.1109/LAWP.2020.2973424.

[28] YANG Xue, XU Shenheng, YANG Fan, *et al*. A novel 2-bit reconfigurable reflectarray element for both linear and circular polarizations[C]. 2017 IEEE International Symposium on Antennas and Propagation & USNC/URSI National Radio Science Meeting, San Diego, USA, 2017: 2083–2084.

[29] KAMODA H, IWASAKI T, TSUMOCHI J, *et al*. 60-GHz electronically reconfigurable large reflectarray using single-bit phase shifters[J]. *IEEE Transactions on Antennas and Propagation*, 2011, 59(7): 2524–2531. doi: 10.1109/TAP.2011.2152338.

[30] LI Long, YANG Yang, and LIANG Changhong. A wide-angle polarization-insensitive ultra-thin metamaterial absorber with three resonant modes[J]. *Journal of Applied Physics*, 2011, 110(6): 063702. doi: 10.1063/1.3638118.

[31] YANG Huanhuan, YANG Fan, CAO Xiangyu, *et al*. A 1600-element dual-frequency electronically reconfigurable reflectarray at X/Ku-Band[J]. *IEEE Transactions on Antennas and Propagation*, 2017, 65(6): 3024–3032. doi: 10.1109/TAP.2017.2694703.

[32] WANG Ke, ZHAO Jie, CHENG Qiang, *et al*. Broadband and broad-angle low-scattering metasurface based on hybrid optimization algorithm[J]. *Scientific Reports*, 2014, 4: 5935.

[33] GUAN Chunsheng, WANG Zhuochao, DING Xumin, *et al*. Coding Huygens' metasurface for enhanced quality holographic imaging[J]. *Optics Express*, 2019, 27(5): 7108–7119. doi: 10.1364/OE.27.007108.

SHUANG Ya, was born in 1993 in Shaanxi, China. She received the B.S. degree from Xidian University, Xi'an, China, in 2016. She is currently pursuing the Ph.D. degree with the Department of Electronics, Peking University, Beijing, China. Her current research interests include metasurface-assisted electromagnetic imaging system, communication system based on information metamaterials, and metasurface design.

E-mail: 1601111240@pku.edu.cn

WANG Zhuo, was born in 1995. He received his B.Eng and M.Eng degree in electronic and information engineering from the Xidian University. He is currently working toward the Ph.D. degree in Peking University. His research interest is intelligent electromagnetic sensing.

E-mail: 2001111254@stu.pku.edu.cn

WEI Menglin, was born in Sep 1995 in Shanxi, China. He received his bachelor's degree from Department of Electronics, Peking University in 2018. He joined State Key Laboratory of Advanced Optical Communication Systems and Networks as a PhD student. He has interests in microwave imaging and reconfigurable intelligent metasurface.

E-mail: wmlpku@pku.edu.cn

LI Lianlin, was born in 1980. He received his Ph.D. degree from the Institute of Electronics, Chinese Academy of Sciences in 2006. He is currently a hundred talented program professor with Peking University. His research interests are super-resolution imaging, microwave imaging, sparse signal processing, and ultrawideband radar systems.

E-mail: lianlin.li@pku.edu.cn